# Along-wind simplified analysis of wind turbines through a coupled blade-tower model

Andrea Spagnoli[*] and Lorenzo Montanari

*Department of Civil-Environmental Engineering and Architecture,
University of Parma, Viale Usberti 181/A, 43124 Parma, Italy*

**Abstract.** A model is proposed to analyse the along-wind dynamic response of upwind turbines with horizontal axis under service wind conditions. The model takes into account the dynamic coupling effect between rotor blades and supporting tower. The wind speed field is decomposed into a mean component, accounting for the well-known wind shear effect, and a fluctuating component, treated through a spectral approach. Accordingly, the so-called rotationally sampled spectra are introduced for the blades to account for the effect of their rotating motion. Wind forces acting on the rotor blades are calculated according to the blade element momentum model. The tower shadow effect is also included in the present model. Two examples of a large and medium size wind turbines are modelled, and their dynamic response is analysed and compared with the results of a conventional static analysis.

**Keywords:** along-wind dynamic response; blade element momentum model; coherent wind speed field; rotationally sampled spectrum; tower shadow effect; upwind horizontal axis wind turbine

## 1. Introduction

In the past three decades the use of wind-powered electrical generators has significantly increased throughout the world. Numerous research studies in different engineering fields have been carried out, leading to a significant improvement in the performances of wind turbines in terms of efficiency of the electric power generation, structural behaviour, noise and so on. For this purpose, devices, such as pitching and braking systems, yaw drives and wind vanes are frequently included in the system. Nowadays the market offers a wide variety of Horizontal Axial Wind Turbines (HAWTs) with two or more blades, ranging from the domestic ones of rotor diameter shorter than 2 m up to huge machines with a rotor diameter of more than 120 m.

In the field of structural engineering, the modelling of wind turbine components, the description of turbolence wind speed field and its interaction with the structure, the dynamic fatigue behaviour of the constituent materials are some of the main topics currently investigated. As far as the simulation of fluctuating component of the wind velocity is concerned, spectral methods are commonly used to describe the statistic characteristics of time variation of wind speed. Purdue (Sundar and Sullivan 1983) and Sandia (Veers 1984) methods defined the stochastic

---

character of the fluctuating wind velocity acting on HAWTs on the basis of Eulerian spectra related to a grid of fixed points in the plane swept by the blades. Connell (1980, 1981), taking into account the rotational motion of the blades, evaluated a so-called rotationally sampled spectrum which derives from the autocorrelation function of the fluctuating wind speed that a point of a rotating blade encounters along its path. In order to perform time-domain dynamic analyses, spectra of turbulence wind speed are commonly processed through the harmonic wave decomposition, implemented in the Fast Fourier Transform (FFT) algorithm (Yang 1972, 1973), while the white noise method is less employed (Powell and Connell 1986). Moreover, the fundamental investigations of Shinozuka (1971) and Shinozuka and Jan (1972), pertaining the simulation of multidimensional and multivariate coherent field of random processes, are commonly applied for describing the characteristics of fluctuating wind speed field.

In dynamic simulations, wind turbines are commonly treated as multi-body structural systems (Murtagh *et al*. 2005, Chen *et al*. 2009). Depending on the desired level of details which has to be achieved, different parts of the wind turbine (blades, drivetrain shaft, yaw bearing hinge, tower, etc.), connected one each other by means of springs, hinges or joints, might be included in the global structural system as single or multi degrees of freedom elements. The use of modal shape functions allows the reduction of the degrees of freedom and in turn of the computational cost. Typically, commercial simulation packages (e.g., the freeware NWTC Design Code FAST, 2013) discretize blade deflection through the first two flapwise eigenmodes and one or two edgewise eigenmodes. However, in order to describe more complex deformation states of flexible wind turbines, full Finite Element (FE) models implementing non-linear beam theories are necessary (Hansen *et al*. 2006).

The correct description of wind-structure interaction in wind turbines requires advanced aerodynamics, and possibly aeroelasticity, concepts. As a matter of fact, conversely to the case of steady structures (e.g., the supporting tower of the wind turbine), the evaluation of wind pressure along the blades requires to account for their relative motion with respect to wind. To this end, the Blade Element Momentum (BEM) model due to Glauert (1935), which is based on momentum conservation and the blade element theory, is often implemented in relevant codes due to its accuracy and computational efficiency. Over the past few years, thanks to the enhancements in the computational methods to solve Eulerian and Navier-Stokes equations, computational fluid dynamics simulation packages have become more and more popular, allowing the modelling of phenomena as complex as those of the interaction between wind generators in wind parks (Hansen *et al*. 2006).

In this paper, a plane FE model is proposed to analyse the along-wind dynamic response of upwind turbines with horizontal axis under service wind conditions. In order to simulate realistically the wind-induced dynamic response of the wind turbine, both the mean and fluctuating wind velocities are considered. A logarithmic law is assumed to describe the wind-shear effect of the mean component, while the fluctuating component of wind speed is described according to the Shinozuka method (Shinozuka *et al*. 1990) used in conjunction with either rotationally sampled spectra for the rotor blades or Eulerian spectra for the tower. The wind turbine is modelled as a two-body (blades and tower) coupled structural system. Due to the higher stiffness of the tower in comparison to that of the blades, the dynamic response of the blades is determined by modelling them as cantilever beams fixedly clamped at the rotor hub. Then the response of the supporting tower is analysed by considering the coupling dynamic effects of the vibrating blades (Murtagh *et al*. 2005, Chen *et al*. 2009). The stiffness of the blades accounts for the geometric effect of radial load which depends on the blade position and the angular frequency (Naguleswaran 1994). The

dynamic equilibrium equations of blades and tower are solved by the Newmark method of constant acceleration (Chopra 1995). The calculation of the aerodynamic loading on the rotating blades is based on the BEM theory (Glauert 1935) modified according to Prandtl (Shen *et al.* 2005) and Buhl (2004) models. The phenomenon of tower shadow, due to the fact that each blade periodically pass in front of the tower is also taken into account in the present model (Bak *et al.* 2001). Finally, two examples of a large and medium size wind turbine are presented, and their dynamic response is analysed and compared with the results of a conventional static analysis in which the rotor blades are assumed to be fixed and the structure to be subjected to a mean wind speed.

## 2. Description of the model

A plane FE model of an upwind HAWT is presented to investigate its along-wind dynamic response. The wind is assumed to blow in the direction of the X-axis (Fig. 1), which is normal to the vertical plane swept by the blades.

The structure of the wind generator is modelled as a two-body coupled system (Fig. 2), constituted by the rotor blades (rotating at a constant angular velocity $\Omega$) and the tower of support. The nacelle and the rotor hub are treated as rigid bodies acting in the model as translational and rotational lumped masses attached to the top of the tower. Due to the higher stiffness of the tower in comparison to that of the blades, their dynamic response is assumed to be independent from tower vibrations. Therefore, the blades are treated as independent rotating cantilever beams fixedly clamped at the rotor hub. The relevant coupling effect of the along-wind blade vibrations on the tower dynamic response (Murtagh *et al.* 2005, Chen *et al.* 2009) is accounted for by treating the tower as a cantilever beam (with a top lumped mass representative of the masses of blades, hub and nacelle) whose free end is submitted to the summation of the fluctuating shear and moment reactions at the blade roots (Fig. 2). The blades and the tower are modelled via Bernoulli-Euler plane beam elements. The spanwise variation, within each finite element, of mass and stiffness properties of blades and tower due to their tapered shape is accounted for by using linear functions.
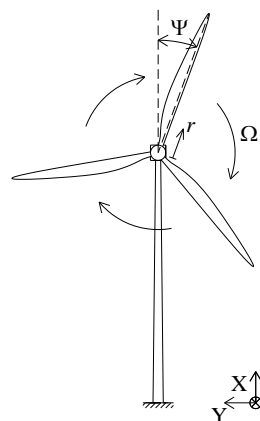


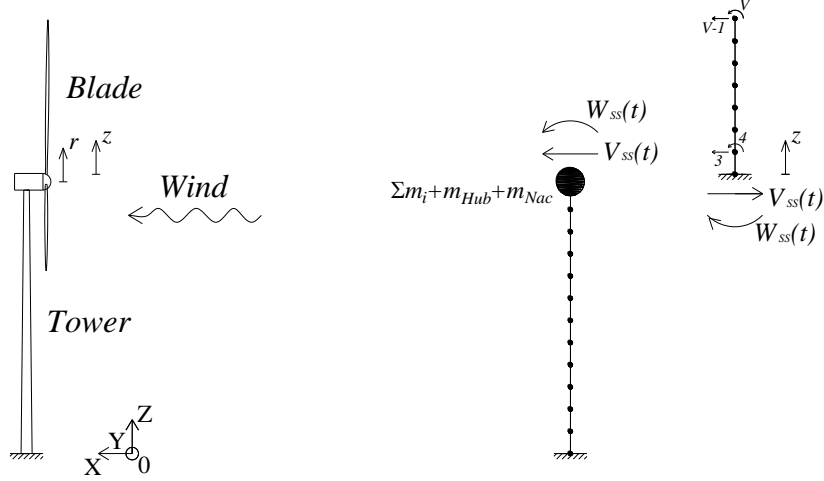Fig. 1 Front view of a three-blade horizontal axis wind turbine

Fig. 2 Side view of the wind turbine and finite element discretization of the coupled blade-tower system, where the *V* degrees of freedom of a single blade are shown along with the blade-tower coupling actions $V_{SS}(t)$ and $W_{SS}(t)$

### *2.1 Dynamic equilibrium of the rotating blades*

According to the adopted FE model, the dynamic equilibrium of each blade can be written in the following discretized form

$$\mathbf{M}_B\ddot{\mathbf{x}}_B + \mathbf{C}_B(t)\dot{\mathbf{x}}_B + \mathbf{K}_B(t)\mathbf{x}_B = \mathbf{F}_B(t) \tag{1}$$

where $\mathbf{M}_B$ is the mass matrix of the blade, $\mathbf{C}_B(t)$ the damping matrix, $\mathbf{K}_B(t)$ the stiffness matrix, $\ddot{\mathbf{x}}_B$, $\dot{\mathbf{x}}_B$ and $\mathbf{x}_B$ are the vectors of the translational and rotational nodal accelerations, velocities and displacements, respectively, and $\mathbf{F}_B(t)$ is the vector of the wind nodal forces acting on the blade at the time *t*. Equation 1 is solved by means of the Newmark step-by-step constant acceleration method (Chopra 1995).

The mass matrix of the blade $\mathbf{M}_B$ is formed by assembling the consistent mass matrices of each finite element (Cook *et al*. 1989). The classical Rayleigh method (Chopra 1995) is employed to build the damping matrix of the blade $\mathbf{C}_B(t)$ as a function of the mass matrix $\mathbf{M}_B$ and the stiffness matrix $\mathbf{K}_B(t)$. The coefficients of the Rayleigh mass matrix are calculated on the basis of the damping ratio at the first two natural frequencies of the blade. The stiffness matrix $\mathbf{K}_B(t)$ is the sum of the elastic stiffness matrix $\mathbf{K}_{E,B}$ and geometric stiffness matrix $\mathbf{K}_{G,B}$, where the latter is obtained by assembling the geometric stiffness matrix of each finite element, $\mathbf{K}_{G,B}^e(t)$, given by

$$\mathrm{K}_{G,B}^e(t) = \int_0^{L^e} \mathrm{G}^T(z')N^e(t,z')\mathrm{G}(z')dz' \tag{2}$$

where $L^e$ is the length of the finite element, $\mathbf{G}(z')$ is the vector of the first derivatives of the

shape functions of the Bernoulli-Euler beam element, $z'$ is the radial coordinate of the finite element, $N^e(t, z')$ is the radial force along the element which is a function of the time $t$. As a matter of fact, such a force is the sum of the two radial forces $N_c^e(z')$ and $N_g^e(t, z')$ due to, respectively, centrifugal action and self-weight of the blade, where the latter is time varying from compression to traction depending on the angular position $\psi$ of the blade. Along the blade, the centrifugal radial force $N_c(z)$ is given by the following expression, function of the $z$-axis originating at the blade root (Fig. 2)

$$N_c(z) = \Omega^2 \int_z^{L_B} \overline{m}(z)\,(R_{Hub} + z)\,dz \tag{3}$$

where $L_B$ is the flexible length of the blade, $\overline{m}(z)$ its mass per unit length and $R_{Hub}$ the radius of the hub. The gravity radial force $N_g(t, z)$ is a function of the angular position $\psi(\psi(t) = \Omega t$, Fig. 1), that is

$$N_g(t, z) = g\cos(\Omega t) \int_z^{L_B} \overline{m}(z)\,dz \tag{4}$$

where $g$ is the gravitational acceleration. It should be noted that, for typical blade geometries and rotational speed, the centrifugal radial force is much higher than the gravity radial force.

The nodal forces $\mathbf{F}_B(t)$ due to wind loading, related to the undisturbed local wind speed estimated by Shinozuka approach (Shinozuka *et al.* 1990) (see Section 2.2 below), are determined through the BEM model described in (Glauert 1935, Shen *et al.* 2005, Buhl 2004) (see Section 2.3 below).

### 2.2 Aft-fore wind speed field acting on the rotating blades

Generally speaking, the undisturbed wind speed field is described by the three components, $u$, $v$, $w$, with respect to the XYZ frame being Z the vertical axis (Fig. 1). Since the along-wind structural response is here investigated, only the u component, characterised by a mean, $\overline{u}$, and a fluctuating, $u'$, term, along the X direction normal to the rotor plane is considered. The wind shear effect dictates the mean wind speed profile along the height $h$, which can be described by the following standard logarithmic expression (Simiu and Scanlan 1996)

$$\overline{u}(h) = \overline{U}_{Hub}\,\ln(h/z_0)/\ln(H_{Hub}/z_0) \tag{5}$$

where $\overline{U}_{Hub}$ is the mean wind speed at the hub height, $H_{Hub}$, and $z_0$ is the surface roughness length of the site. The height at the $r$ coordinate of the $i$-blade is given by the following time-varying function

$$h(r, t) = H_{Hub} + r\cos(\Omega t + \varphi_i) \tag{6}$$

Where $\varphi_i$ is the initial phase angle of the $i$-blade.

The fluctuating component $u'(t)$ of the wind speed field is herein treated statistically through appropriate power spectral density functions of turbulence. As has been explained by Connell (1980), the spectrum of turbulence encountered by a rotating point on the blade, the so-called rotationally sampled spectrum, can be quite different from that observed by a fixed point.

Depending on the atmospheric gust characteristics, the rotational velocity and the distance of the rotating point from the centre of rotation, the energy content of such a spectrum is shifted from mid frequencies to high frequencies corresponding to multiples of the rotational frequency on the blades. Then according to the PNL method (Powell *et al.* 1985), the autocorrelation function $R_{jj}(\tau)$ of the turbulence component of the wind speed, $u'_j(t)$, encountered by the *j*-node rotating at a constant velocity $\Omega$ and with a distant *r* from the centre of the hub, is given by

$$R_{jj}(\tau) = \frac{2\,\sigma^2}{\Gamma(1/3)}\left[\alpha_j^2 \sin^2\left(\frac{\Omega\tau}{2}\right) + \beta^2\left(\frac{\Omega\tau}{2}\right)^2\right]^{1/6} (P-Q) \tag{7}$$

where

$$P = K_{1/3}\left\{2\left[\alpha_j^2 \sin^2\left(\frac{\Omega\tau}{2}\right) + \beta^2\left(\frac{\Omega\tau}{2}\right)^2\right]^{1/2}\right\} \tag{8}$$

and

$$Q = \frac{\alpha_j^2 \sin^2\left(\dfrac{\Omega\tau}{2}\right)}{\left[\alpha_j^2 \sin^2\left(\dfrac{\Omega\tau}{2}\right) + \beta^2\left(\dfrac{\Omega\tau}{2}\right)^2\right]^{1/2}} K_{2/3}\left\{2\left[\alpha_j^2 \sin^2\left(\frac{\Omega\tau}{2}\right) + \beta^2\left(\frac{\Omega\tau}{2}\right)^2\right]^{1/2}\right\} \tag{9}$$

and $\tau$ = correlation time; $\sigma^2$ = variance of the u-component turbulence; $\Gamma$ = gamma function; $\alpha_j^2 = (R_{Hub} + z_j)/L_{u,y}$, where $L_{u,y}$ is the integral length scale of the u-component in the cross-wind direction; $\beta = \overline{U}_{Hub}/(\Omega L_{u,x})$, where $L_{u,x}$ is the integral length scale of the u-component in the along-wind direction; $K_\nu$ = modified Bessel function of the second kind of fractional order $\nu$.

According to (Simiu and Scanlan 1996), the standard deviation of the turbulence, $\sigma$, is assumed to be proportional (by a factor function of $z_0$) to the friction velocity $u_*$ which is described by the following expression

$$u_* = \frac{k\,u(h)}{\ln\left(\dfrac{h}{z_0}\right)} \tag{10}$$

where $k$ = von Kármán constant (typically equal to about 0.4). According to Wiener-Khintchine (Shinozuka 1971) using the Fourier transform of the autocorrelation function $R_{jj}(\tau)$, the corresponding two-side auto-Power Spectral Density Function (auto-PSDF) is evaluated

$$S_{jj}(\omega_k) = \frac{1}{2\pi}\int_{-\infty}^{+\infty} R_{jj}(\tau)e^{-i\omega\tau}d\tau = \frac{1}{\pi}\int_0^{\infty} R_{jj}(\tau)\cos(\omega_k\tau)d\tau \tag{11}$$

Where $\omega_k$ is the sampled pulsation equal to $\Delta\omega, 2\Delta\omega, ..., k\Delta\omega, ...K\Delta\omega$ ( $\Delta\omega = 2\pi/T$, with $T =$

duration of the signal assumed to be periodic, is the minimum pulsation and $K\Delta\omega$ is the maximum pulsation being considered).

In order to account for the spatial coherence of the fluctuating wind speed field, the signals of the wind speed at the blade nodes are spatially correlated with that at the hub centre. Such a signal coherence decreases with increasing distance between nodes. Davenport coherence function $\gamma_{jl}$ for fluctuating wind speeds $u'_j(t)$ and $u'_l(t)$ at the nodes $j$ and $l$, respectively, is approximately assumed to be equal to (Davenport 1968)

$$\gamma_{jl}(\omega_k) = e^{-\frac{\omega_k C \Delta_{jl}}{2\pi \overline{U}_{Hub}}} \tag{12}$$

where $C$ is the coherence decay constant (Simiu and Scanlan 1996), $\Delta_{jl}$ is the distance between the nodes $j$ and $l$.

The fluctuating wind speed field $u'$ is described as a one-dimensional multivariate homogeneous Gaussian coherent stationary random process with zero mean value through the harmonic superposition method of Shinozuka (Shinozuka *et al.* 1990)

$$u'_j(t) = 2\sqrt{\Delta\omega} \sum_{l=1}^{j} \sum_{k=1}^{K} |H_{jl}(\omega_k)| \cos[\omega_k t + \theta_{jl}(\omega_k) + \Phi_{lk}] \quad j = 1, 2, \ldots, J+1 \tag{13}$$

where $J+1$ is the total number of nodes where the aerodynamic forces are evaluated (corresponding to the nodes of the FE discretization) including the hub centre, $\Phi_{lk}$ is the independent random phase angle uniformly distributed between 0 and $2\pi$, and $\theta_{jl}(\omega_k)$ is the angle explained in Eq. (18) below.

The quantity $H_{jl}(\omega_k)$ is the $jl$-term of the lower triangular matrix $\mathbf{H}(\omega_k)$ obtained by the Cholesky decomposition of the two-side cross-power spectral density matrix $\mathbf{S}(\omega_k)$ of the process, namely

$$\mathbf{S}(\omega_k) = \mathbf{H}(\omega_k)\mathbf{H}^T(\omega_k) \tag{14}$$

or

$$\mathbf{S}(\omega_k) = \begin{bmatrix} S_{11} & & & & & \\ \vdots & \ddots & & & sym & \\ \vdots & \vdots & S_{jj} & S_{jl} & & \\ \vdots & \vdots & S_{lj} & S_{ll} & & \\ \vdots & \vdots & \vdots & \vdots & \ddots & \\ S_{J+1\,1} & \cdots & \cdots & \cdots & \cdots & S_{J+1\,J+1} \end{bmatrix} \tag{15}$$

The diagonal terms $S_{jj}(\omega_k)$, corresponding to the values of the auto-PSDF at the pulsation $\omega_k$, are obtained for $j = 2, \ldots, J+1$ from the rotationally sampled spectra of the $J$ nodes along the blade. The auto-PSDF $S_{11}(\omega_k)$ corresponds to the two-side Eulerian von Kármán spectrum at the hub centre

$$S_{11}(\omega_k) = \frac{\sigma^2 L_{u,x}/\overline{U}_{Hub}}{\pi[1 + (1.399\omega_k L_{u,x}/\overline{U}_{Hub})^2]^{5/6}} \quad (16)$$

The off-diagonal terms $S_{jl}(\omega_k)$ are the cross-PSDFs, representing the spatial coherence of the wind speed field, which are determined as a function of the auto-PSDFs and of the coherence function $\gamma_{jl}$ of Eq. (12) through the following expression

$$S_{jl}(\omega_k) = \sqrt{S_{jj}(\omega_k)S_{ll}(\omega_k)}\ \gamma_{jl}(\omega_k) \quad (17)$$

Finally, the angle $\theta_{jl}(\omega_k)$ appearing in Eq. (13) is obtained from the term $H_{jl}(\omega_k)$ as follows

$$\theta_{jl}(\omega_k) = \arctan\left\{\frac{\text{Im}[H_{jl}(\omega_k)]}{\text{Re}[H_{jl}(\omega_k)]}\right\} \quad (18)$$

Fig. 3 shows an illustrative example of the PSDF for a fixed point at the hub centre (von Kármán spectrum) and for rotating points at different radial positions (rotationally sampled spectra). As has been suggested by Yang (1972, 1973), FFT technique is here employed to reduce drastically the computational cost in generating the time-histories of the fluctuating wind speed field.
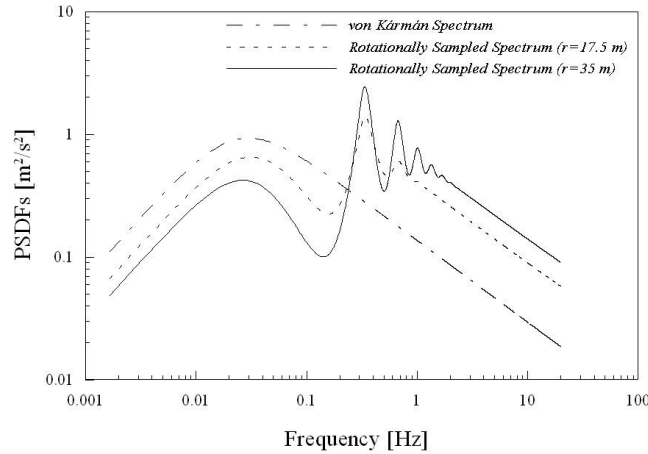


Fig. 3 Example of power spectral density functions of fluctuating wind speed at the hub height (von Kármán spectrum) and at two points along the rotating blade (rotationally sampled spectrum) at a distance of 17.5 m and 35 m from the hub centre ( $\overline{U}_{Hub} = 15m/s$ , $L_{u,x} = L_{u,y} = 73.5m$ , $\sigma^2 = 2.19m^2/s^2$ and $\Omega = 2.07\ rad/s$ )

## 2.3 Aerodynamics wind loads acting on the rotating blades

Owing to the relative motion of blades with respect to the undisturbed wind speed field, the estimation of the aerodynamics wind loads acting on the rotating blades is a difficult task. The

fundamental BEM theory (Glauert 1935), modified by Prandtl model (Shen *et al.* 2005) and Buhl's (2004), is here applied to determine the elementary along-wind force $dF_B$ acting on the blade element of length dr, located at a distant r from the hub centre

$$dF_B = \frac{1}{2} C_{N,A} \rho u_{rel}^2 c dr \tag{19}$$

where $\rho$ is the air density and c the length of the local cross section chord (Fig. 4). The coefficient $C_{N,A}$, $C_{N,A} = C_l \cos\phi + C_d \sin\phi$ is the local normal aerodynamic coefficient, where $C_l = C_l(\alpha)$ and $C_d = C_d(\alpha)$ are, respectively, the static lift and the drag coefficients, function of the attack angle $\alpha$, $\alpha = \phi - \beta$ (see Fig. 4), with $\phi$ being the inflow angle of the relative wind velocity $u_{rel}$ (see below) and $\beta$ is the local pitch angle sum of the blade pitch angle and of the local twist angle. The coefficients $C_l$ and $C_d$ are commonly given in a tabular form for standardized airfoil sections. As is shown in Fig. 4, the local relative wind velocity $u_{rel}$ is equal to $\sqrt{[u(1-a)]^2 + [\Omega r(1+a')]^2}$, where $u$ is the undisturbed local inflow wind speed, sum of the mean and the fluctuating components. The coefficients $a$ and $a'$ are the axial and tangential induction factors representative of the variation of the axial and tangential local wind velocities, respectively, due to wake effects induced by the turbine. These coefficients are calculated through the following semi-empirical expressions (Buhl 2004)

$$a = \begin{cases} \left[ \dfrac{4F \sin^2\phi}{\sigma'(C_l \cos\phi + C_d \sin\phi)} + 1 \right]^{-1}, & C_T \leq 0.96F \\[4mm] \dfrac{18F - 20 - 3\sqrt{C_T(50 - 36F) + 12F(3F - 4)}}{36F - 50}, & C_T > 0.96F \end{cases} \tag{20}$$

and

$$a' = \left[ \frac{4F \sin\phi \cos\phi}{\sigma'(C_l \sin\phi - C_d \cos\phi)} - 1 \right]^{-1} \tag{21}$$

The thrust coefficient $C_T$ of the pressure on the element is given by

$$C_T = \frac{\sigma'(1-a)^2(C_l \cos\phi + C_d \sin\phi)}{\sin^2\phi} \tag{22}$$

where $\sigma' = Bc/(2\pi r)$ is the local solidity and $B$ is the number of blades. The loss factor $F$ due to Prandtl model (Shen *et al.* 2005) accounts for the effect of the vortex shedding at the blade tip and near the rotor hub on the induced velocity

$$F = F_{Hub} F_{Tip} \tag{23}$$

where

$$F_{Hub} = \frac{2}{\pi} \arccos \left[ e^{-\frac{B(r-R_{Hub})}{2R_{Hub}\sin\phi}} \right] \qquad (24)$$

and

$$F_{Tip} = \frac{2}{\pi} \arccos \left[ e^{-\frac{B(L_B+R_{Hub}-r)}{2r\sin\phi}} \right] \qquad (25)$$

An iterative procedure is required to calculate the induced factors of Eqs. (20) and (21) (Dai *et al*. 2011). The Newton-Raphson method is here employed together with the adjustments proposed by Maniaci (2011) in order to overcome convergence issues of the BEM method.

Finally, the influence of the presence of the tower behind the rotor blades on the local wind speed field, called the tower shadow effect, is considered in the proposed model. Bak method (Bak *et al*. 2001), proposed for upwind HAWTs, is adopted. Accordingly, the correction multiplication factor of the undisturbed local inflow wind speed *u* is

$$f_{ts} = 1 - \frac{(x'+0.1)^2 - y'^2}{\left[(x'+0.1)^2 + y'^2\right]^2} + \frac{C_{d,T}}{2\pi} \frac{x'+0.1}{(x'+0.1)^2 + y'^2} \qquad (26)$$

where $x'$ and $y'$ are, respectively, the upwind and crosswind distance of the blade axis from the tower midline normalized with respect to the tower radius at the height of interest; $C_{d,T}$ is the drag coefficient of the tower function of Reynolds number, here calculated for local mean speed according to Eq. (5).
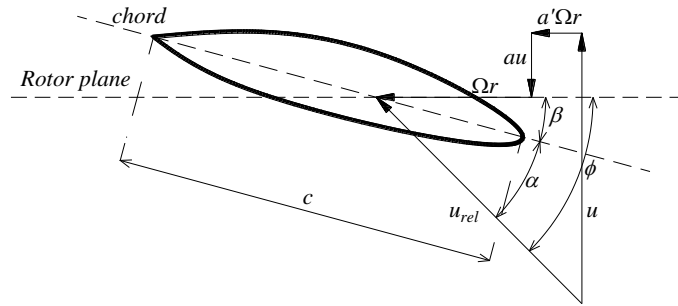


Fig. 4 Airfoil section of the blade and relevant aerodynamic angles for BEM theory

## 2.4 Dynamic equilibrium of the coupled tower-blade system

While the dynamic response of the blades is virtually independent of the deflections undergone by the supporting tower of the wind turbine, the dynamic response of the tower itself might significantly be influenced by the vibration of blades (Murtagh *et al*. 2005, Chen *et al*. 2009). To account for this coupling phenomenon, the overtop system of the wind turbine supported by the

tower is considered by including into the dynamic equilibrium equations of the tower the translational and rotational masses related to the superstructure (blades, hub and nacelle), $\mathbf{M}_{SS}$, lumped at the tower top (see Eq. (28) below), and the vector, $\mathbf{F}_{SS}(t)$, containing the moment and the shear dynamic reactions of the blades at their roots (see Eq. (29) below). Then, the along-wind response of the tower is evaluated by solving the dynamic equilibrium equations of the coupled system through the Newmark step-by-step constant acceleration method (Chopra 1995)

$$(\mathbf{M}_T + \mathbf{M}_{SS})\ddot{\mathbf{x}}_T + \mathbf{C}_T\,\dot{\mathbf{x}}_T + \mathbf{K}_T\,\mathbf{x}_T = \mathbf{F}_T(t) + \mathbf{F}_{SS}(t) \tag{27}$$

where $\mathbf{M}_T$ is the mass matrix of the tower, $\mathbf{C}_T$ the damping matrix of the tower constructed by the Rayleigh method (Chopra 1995), $\mathbf{K}_T$ the elastic stiffness matrix of the tower, $\mathbf{F}_T(t)$ the wind forces acting on the tower, $\ddot{\mathbf{x}}_T$, $\dot{\mathbf{x}}_T$ and $\mathbf{x}_T$ the vectors of the translational and rotational nodal accelerations, velocities and displacements, respectively, of the tower, discretized by means of the plane Bernoulli-Euler beam elements.

The mass matrix of the superstructure, $\mathbf{M}_{SS}$, is given by

$$\mathbf{M}_{SS} = \begin{bmatrix} 0 & & & & & \\ \vdots & \ddots & & & sym & \\ \vdots & \vdots & \ddots & & & \\ \vdots & \vdots & \vdots & 0 & & \\ \vdots & \vdots & \vdots & \vdots & \sum_{i=1}^{B}(m_i) + m_{Hub} + m_{Nac} & \\ 0 & \cdots & \cdots & \cdots & 0 & \left[\sum_{i=1}^{B}(m_i) + m_{Hub}\right]\Delta_{TH}^2 + m_{Nac}\Delta_{TN}^2 \end{bmatrix} \tag{28}$$

where $m_i$ is the mass of the $i$-blade, $m_{Hub}$ is the mass of the hub, $m_{Nac}$ is the mass of the nacelle, $\Delta_{TH}$ is the distance between the tower top and the hub centre of mass, $\Delta_{TN}$ is the distance between the tower top and the nacelle centre of mass. The vector $\mathbf{F}_{SS}(t)$ of the shear force and moment transmitted into the tower top is

$$\mathbf{F}_{SS}(t) = \begin{Bmatrix} 0 \\ \vdots \\ \vdots \\ 0 \\ V_{SS}(t) \\ W_{SS}(t) \end{Bmatrix} \tag{29}$$

The shear force resultant of the dynamic response of the superstructure is given by

$$V_{SS}(t) = \sum_i \sum_j \sum_k K_{B,jk}^{(i)}(t) x_{B,k}^{(i)}(t) + F_{Hub}(t) \qquad \begin{cases} i = 1,2,\ldots,B \\ j = 3,5,\ldots,V-1 \\ k = 3,4,\ldots,V \end{cases} \tag{30}$$

Where $K_{B,jk}^{(i)}(t)$ is the *jk*-term of the stiffness matrix (related to the *j*-th translational degree of freedom) of the *i*-blade, $x_{B,k}^{(i)}(t)$ is the general *k*-th translational/rotational degree of freedom of the *i*-blade. The force $F_{Hub}(t) = \frac{1}{2}C_{d,Hub}\rho R_{Hub}^2[\overline{U}_{Hub} + U'_{Hub}(t)]^2$ is the aerodynamic wind load acting on the hub where $C_{d,Hub}$ is the drag aerodynamic coefficient of the hub and $U'_{Hub}(t)$ is the fluctuating velocity at the hub.

Then the moment resultant of the dynamic response of the superstructure is

$$W_{SS}(t) = \sum_i \sum_j \sum_k K_{B,jk}^{(i)}(t) x_{B,k}^{(i)}(t) \Delta_k^{(i)} + \sum_i \sum_h \sum_k K_{B,hk}^{(i)}(t) x_{B,k}^{(i)}(t) + F_{Hub}(t)\Delta_{TH} \begin{cases} i = 1,\ldots,B \\ j = 3,5,\ldots,V-1 \\ k = 3,4,\ldots,V \\ h = 4,6,\ldots,V \end{cases} \quad (31)$$

Where $K_{B,hk}^{(i)}(t)$ is the *hk*-term of the stiffness matrix (related to the *h*-th rotational degree of freedom) of the *i*-blade and $\Delta_k^{(i)}$ is the distance between the node corresponding to the *k*-degree of freedom of the *i*-blade and the node at $z = 0$ (Fig. 2).

### 2.5 Aft-fore wind speed field acting on the tower

The *u*-component of the wind speed acting on the tower along the X-axis is decomposed into the mean and fluctuating terms. The former term is described according to Eq. (5) to account for wind shear effect. The fluctuating wind speed field is generated so as to consider a spatial correlation of the nodal wind loads along the height of the tower. The following Eulerian von Kármán spectrum is employed

$$S_{VK}(\omega_k) = \frac{\sigma^2 L_{u,x}/\overline{u}}{\pi[1 + (1.399\omega_k L_{u,x}/\overline{u})^2]^{5/6}} \quad (32)$$

Due to the specific wind speed profile along the height of the tower, each node is characterized by a different spectrum since the mean wind speed $\overline{u}$ is a function of the height. Shinozuka formulas (see Eqs. (13)-(18)) are applied considering the vertical coherence of the wind speed field through the following Davenport coherence function $\gamma_{jl}$ (Davenport 1968) between the two nodal points *j* and *l*

$$\gamma_{jl}(\omega_k) = e^{-\frac{\omega_k C \Delta_{jl}}{\pi(\overline{u}_j + \overline{u}_l)}} \quad (33)$$

It has to be underlined that, in order to capture the real frequency content of the fluctuating wind speed acting on the blades, rotationally sampled spectra have been used. This has the drawback of requiring the generation of two independent wind speed fields, one for the blades and the other one for the tower, which are coherent one each other solely with respect to the wind speed at the hub centre.

## 3. Illustrative examples

For illustrative purposes, the proposed model is here employed to simulate the dynamic response of two upwind wind-powered electrical generators, called WindPACT 1.5 MW and AOC 15/50. The adopted aerodynamic and mechanical characteristics of the blades and tower of the two wind turbines are the same as those reported in the benchmark models of (NWTC Design Code FAST 2010). The WindPACT 1.5MW is a large size turbine characterized by a three-blade rotor with a diameter of 70 m. The hub is located at a height of 84 m on the ground and has a diameter of 3.5 m. The blade rotational frequency is equal to 0.33 Hz. The damping ratios of the first two natural frequencies of the blade are assumed to be equal to 3.9%. The masses of each blade, hub and nacelle are equal to 4356 kg, 15148 kg and 51170 kg, respectively. The supporting steel tower has a tapered shape with height equal to 82.39 m. Its first two damping ratios are assumed to be equal to 3.4%. The AOC 15/50 HAWT is a medium-size wind turbine having a three-blade rotor with a diameter of 14.98 m. The hub is located at a height of 25 m on the ground and has a diameter of 0.56 m. The blade rotational frequency is equal to 1.07 Hz. The damping ratios of the first two natural frequencies of the blade are assumed to be equal to 4%. The masses of each blade, hub and nacelle are 139 kg, 247 kg and 1747 kg, respectively. The supporting steel tower has a tapered shape with height equal to 24.4 m. Its first two damping ratios are assumed to be equal to 3%. The selected values of the damping ratios are typical for the blade and tower structures under consideration. The adopted finite element discretizations for blades and tower in the two wind turbines are the same as those reported in the benchmark models of (NWTC Design Code FAST, 2010). More in details, 10 elements along each blade and 10 elements along the tower are used in the AOC 15/50 turbine, while 20 elements along each blade and 9 elements along the tower are used in the WindPACT 1.5 MW turbine.

The following parameters are used to describe the undisturbed wind speed field: mean wind speed at the hub height, $\overline{U}_{Hub}$, equal to 15 m/s; surface roughness length, $z_0$, equal to 0.03; integral length scales of the u-component in the along-wind, $L_{u,x}$, and cross-wind, $L_{u,y}$, direction equal to 73.5 m; air density, $\rho$, of 1.225 kg/m$^3$; kinematic air viscosity of $1.4639 \cdot 10^{-5}$ m$^2$/s; coherence decay constant, $C$, equal to 8.8. The standard deviation of the fluctuating wind speed is assumed to be equal to $\sqrt{6}u_*$ (see Eq. (10) for $u_*$) (Simiu and Scanlan 1996). Wind speed spectra with a maximum frequency of 20 Hz are considered to generate wind speed time-histories having a duration of 120 sec. For the dynamic analyses an integration time step of 0.012 sec is assumed. As an example, in Fig. 5 the time-history of the u-component of the wind speed at the hub centre, used in the ensuing simulation of WindPACT 1.5 MW, is presented.
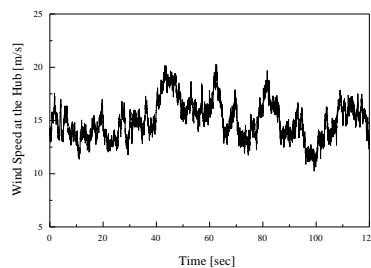


Fig. 5 Sample of generated time-history of wind speed at the hub height of WindPACT 1.5 MW wind turbine

In Table 1, the relevant along-wind natural frequencies of the two wind turbines along with their rotational frequencies are reported. The blade natural frequencies are obtained by an eigenvalue analysis of a single blade, where the stiffness matrix is formed by considering only the geometric contribution due to centrifugal forces. As for the tower, the eigenvalue analysis is performed on the basis of the elastic stiffness matrix of the tower, $\mathbf{K}_T$, and its mass matrix, $\mathbf{M}_T + \mathbf{M}_{SS}$ (see Eq. (28)).

The results of the dynamic analyses for the two wind turbines being considered are presented in terms of the time history of the following along-wind quantities: displacement at the blade tip and at the tower top, and shear force at the blade root and at the tower base. The results are normalised with respect to those obtained from a static analysis of the turbines with fixed blades (park condition) and subjected to a mean wind speed. The static displacement at the blade tip refers to an horizontal blade position ($\Psi=90°$, Fig. 1). The results of the static analyses are shown in Table 2.

Table 1 Summary of the dominant frequencies for the two analysed wind turbines

|  | *WindPACT 1.5 MW* | *AOC 15/50* |
|---|---|---|
| *Blade rotational frequency* [Hz] | 0.33 | 1.07 |
| *Blade 1st natural frequency* [Hz] | 1.32 | 4.26 |
| *Blade 2nd natural frequency* [Hz] | 3.77 | 13.88 |
| *Tower 1st natural frequency* [Hz] | 0.42 | 1.65 |
| *Tower 2nd natural frequency* [Hz] | 3.00 | 12.04 |

Table 2 Results of the static analysis for the two analysed wind turbines under park conditions and mean wind speed

|  | *WindPACT 1.5 MW* | *AOC 15/50* |
|---|---|---|
| *Blade tip displacement* [m] | 0.229 | 0.015 |
| *Blade root shear force* [kN] | 14.81 | 0.75 |
| *Tower top displacement* [m] | 0.074 | 0.008 |
| *Tower base shear force* [kN] | 63.70 | 3.35 |

The time histories of the dynamic responses of WindPACT 1.5 MW and AOC 15/50 are reported in Figs. 6-9 and Figs. 10-13, respectively. All the time histories reported exhibit an initial transient stage followed by a steady state stage. For the displacement at the tower top, a comparison with the results obtained by the FAST code (NWTC Design Code FAST 2010), where the whole blade-tower structural system is modelled, is presented in Figs. 8 and 12. It can be seen that the comparison is in general satisfactory with a slightly smaller average value predicted by FAST in comparison to that of the present model in the case of the WindPACT turbine.

Firstly, it can be observed that, under the same wind speed conditions, the amplification of both deflection and shear with respect to the static values is significant, and turns out to be greater in the large-size turbine than in the medium-size counterpart. Such an amplification is mainly due to the effect both of blade rotational motion on aerodynamics pressures and of inertial forces. For instance, the average normalized displacement at the blade tip is about 12.1 and 5.4 times higher

than the static value in WindPACT 1.5 MW and AOC 15/50, respectively. For the displacement at the tower top such an amplification factor becomes equal to about 9.3 and 3.0 in WindPACT 1.5 MW and AOC 15/50, respectively. Moreover, the amplitudes of displacement/shear vibrations in the steady state stage tend to be higher in the case of WindPACT 1.5 MW as compared to those related to AOC 15/50. For instance, the largest amplitude of vibration for the normalised displacement at the blade tip is equal to about 2.5 and 0.8 in WindPACT 1.5 MW and AOC 15/50, respectively.
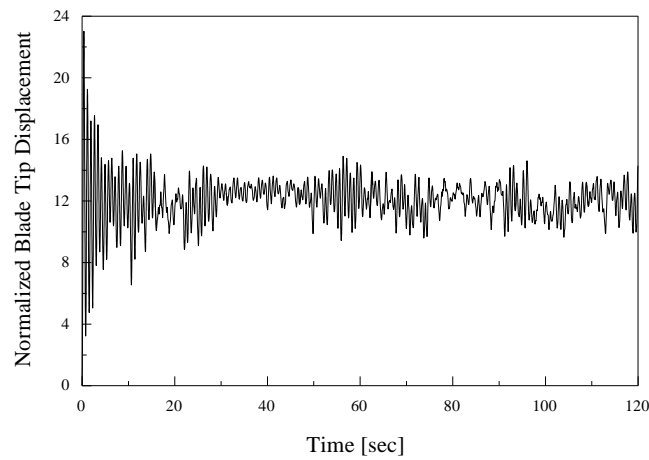


Fig. 6 Time-history of the normalised along-wind displacement at the blade tip of WindPACT 1.5 MW wind turbine
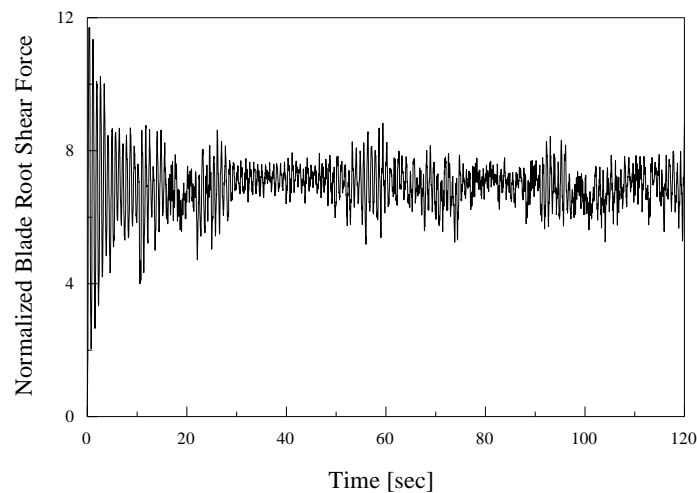


Fig. 7 Time-history of the normalised along-wind shear force at the blade root of WindPACT 1.5 MW wind turbine
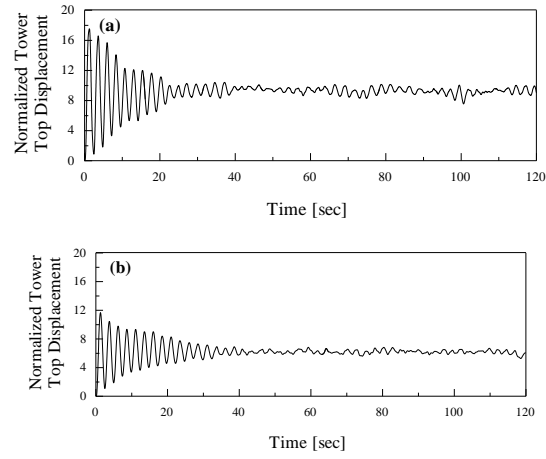
Fig. 8 Time-history of the normalised along-wind displacement at the tower top of WindPACT 1.5 MW
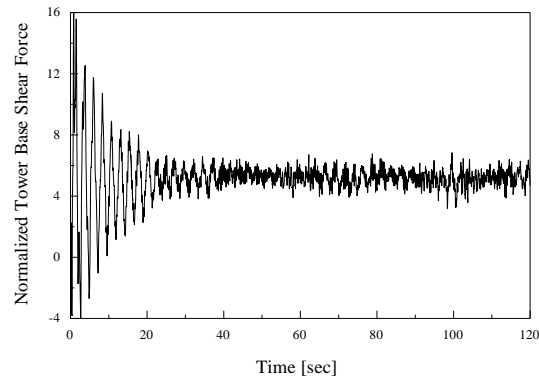     wind turbine: (a) present model and (b) FAST code



Fig. 9 Time-history of the normalised along-wind shear force at the tower base of WindPACT 1.5 MW
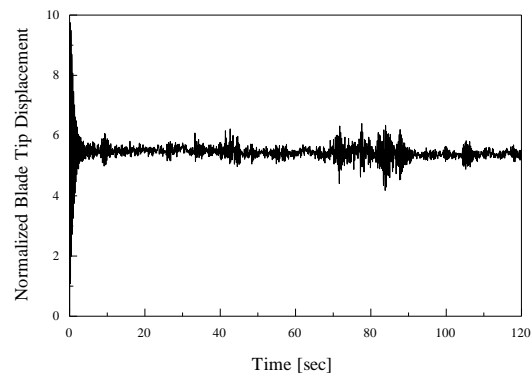     wind turbine



Fig. 10 Time-history of the normalised along-wind displacement at the blade tip of AOC 15/50 wind
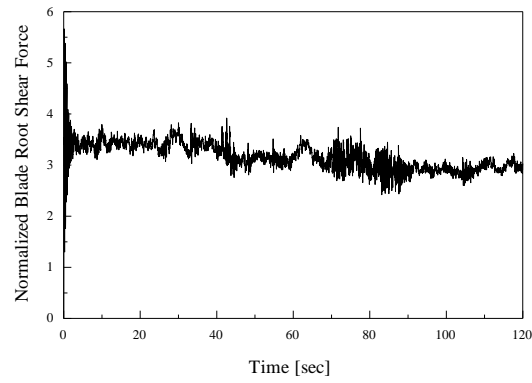     turbine

Fig. 11 Time-history of the normalised along-wind shear force at the blade root of AOC 15/50 wind turbine
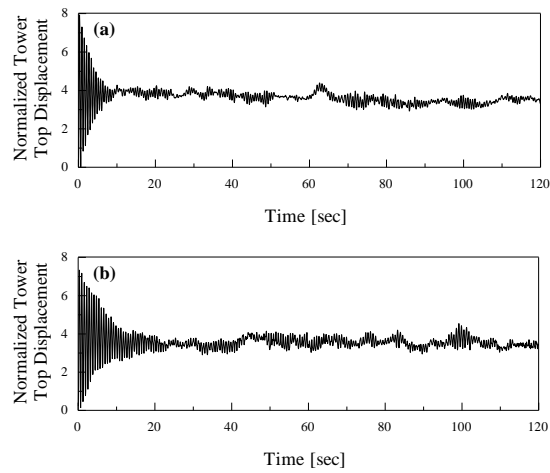


Fig. 12 Time-history of the normalised along-wind displacement at the tower top of AOC 15/50 wind turbine: (a) present model and (b) FAST code
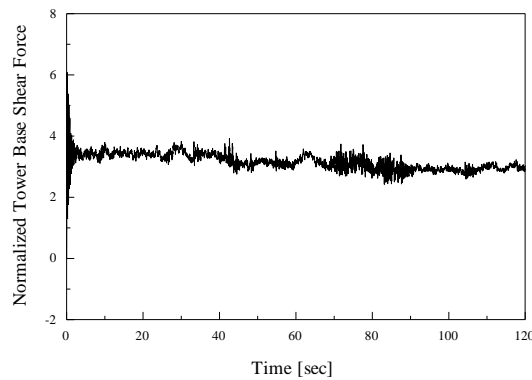


Fig. 13 Time-history of the normalised along-wind shear force at the tower base of AOC 15/50 wind turbine
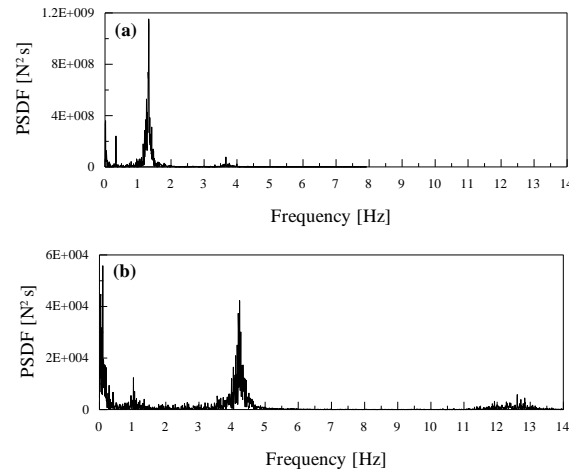
Fig. 14 Power spectral density function of the shear force at the blade root: (a) WindPACT 1.5 MW wind turbine and (b) AOC 15/50 wind turbine
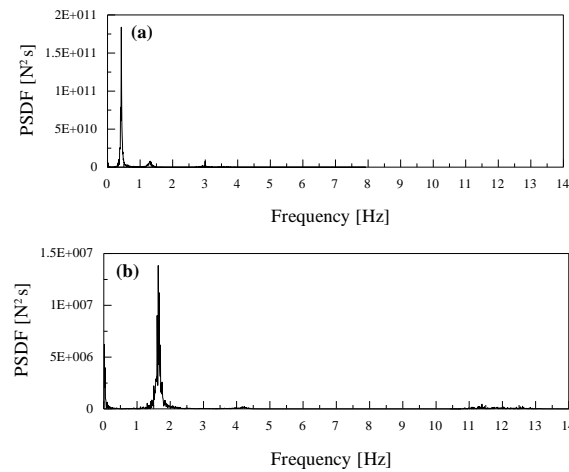


Fig. 15 Power spectral density function of the shear force at the tower base: (a) WindPACT 1.5 MW wind turbine and (b) AOC 15/50 wind turbine

Finally, the time-histories of the displacement at the blade tip and those of the shear at the blade root show dominant frequencies corresponding to the first two natural frequencies of the blades and to the rotational frequency of the rotor. This trend is shown in the FFT results reported in Fig. 14 for the shear at the blade root. As far as the supporting tower is concerned, its dynamic response shows the effect of blade-tower coupling. In fact, the dominant frequencies are in the correspondence of the fundamental natural frequencies of the blades (this points out the blade dynamic flapping action transmitted into the tower) and of the first two natural frequencies of the tower (see the FFT results of Fig. 15 for the shear at the tower base).

## 4. Conclusions

In this paper a plane FE model is presented to perform time-domain along-wind dynamic analyses of upwind HAWTs. The structure is modelled as a coupled two-body system constituted by the blades and the tower of support, where the response of the tower is analysed by considering the coupling dynamic effects of the vibrating blades. The stiffness of the blades accounts for the geometric effect of radial load due to self-weight and centrifugal forces. Mean and fluctuating components are considered to simulate the two spatially coherent wind speed fields acting on the blades and on the tower. For a rigorous evaluation of the aerodynamic loading on the rotating blades, rotationally sampled spectra, BEM model and tower shadow effect are taken into account.

Two wind turbines having different sizes are modelled and their dynamic response is investigated. The results clearly show a significant amplification of displacements in comparison to those of a static analysis where the blades are fixed and a mean wind pressure is considered. This behavioural trend, which is more evident for large-size wind turbines, demonstrate that the use of simplified static analyses might strongly underestimate the stress level in the structure. In addition, the forced vibration of the supporting tower submitted to the sum of the shear forces at the blade roots might lead to a dynamic along-wind response characterised by dominant frequencies related to the blade first natural frequency and the main natural frequencies of the tower. This outcome clearly indicates a blade-tower coupling effect which is neglected when the wind turbine is designed by treating the tower and rotor as separate systems.

In conclusion, the proposed model, despite its relative simple features in comparison to more sophisticate methods, might be a useful tool for preliminary design and qualitative analysis into the along-wind dynamic interaction effects undergone by wind turbines under service conditions, which might lead to additional detailed and optimized analyses.

## References

Bak, C., Madsen, A.H. and Johansen, J. (2001), "Influence from blade-tower interaction on fatigue loads and dynamics", *Proceedings of the 2001 European wind energy conference and exhibition,* Copenhagen, July.

Buhl, M.L. Jr. (2004), *A new empirical rlationship between trust coefficient and induction factor for the turbulent windmill state*, *NREL/TP-500-36834*. Golden, CO: National Renewable Energy Laboratory.

Chen, X., Li, J. and Chen, J. (2009), "Wind-induced response analysis of a wind turbine tower including the blade-tower coupling effect", *J. Zhejiang University*, **10**(11), 1573-1580.

Chopra, A.K. (1995), *Dynamics of structures*, *Theory and Applications to Earthquake Engineering*, Prentice Hall, Englewood Cliffs, NJ.

Connell, J.R. (1980), *Turbulence spectrum observed by a fast-rotating wind turbine blade*, Technical report PNL-3426[R], Richland, WA: Batelle Pacific Northwest Laboratory.

Connell, J.R. (1981), *The spectrum of wind speed fluctuations encountered by a rotating blade of a wind energy conversion system*, *Technical report PNL-4083[R]*, Richland, WA: Batelle Pacific Northwest Laboratory.

Cook, R.D., Malkus, D.S. and Plesha, M.E. (1989), *Concepts and applications of the finite element analysis*, John Wiley & Sons, New York.

Dai, J.C., Hu, Y.P., Liu, D.S. and Long, X. (2011), "Aerodynamic loads calculation and analysis for large scale wind turbine based on combining BEM modified theory with dynamic stall model", *Renew. Energ*., **36**, 1095-1104.

Davenport, A.G. (1967), "The dependence of wind load upon meteorological parameters", *Proceedings of the International Research Seminar on Wind Effects on Buildings and Structures,* Ottawa, September.

FAST (2013), *NWTC design codes FAST*, Golden, CO.

Glauert, H. (1935), *Airplane Propellers*, Aerodynamic Theory, (Ed. W. F. Durand), Berlin.

Hansen, M.O.L., Sørensen, J.N., Voutsinas, S., Sørensen, N. and Madsen, H.A. (2006), "State of the art in wind turbine aerodynamics and aeroelasticity", *Prog. Aerosp. Sci.*, **42**(4), 285-330.

Maniaci, D.C. (2011), "An investigation of WT perf convergence issues", *Proceedings of the 49th AIAA Aerospace Sciences Meeting and Exhibit*, Orlando, FL, January.

Murtagh, P.J., Basu, B. and Broderick, B.M. (2005), "Along-wind response of a wind turbine tower with blade coupling subjected to rotationally sampled wind loading", *Eng. Struct.*, **27**(8), 1209-1219.

Naguleswaran, S. (1994), "Lateral vibration of a centrifugally tensioned uniform Euler-Bernoulli beam", *J. Sound Vib.*, **176**(5), 613-624.

Powell, D.C., Connell, J.R. and George, R.L. (1985), Verification of theoretically computed spectra for a point rotating in a vertical plane, *Technical report PNL-5440[R]*. Richland, WA: Battelle Pacific Northwest Laboratory.

Powell, D.C. and Connell, J.R. (1986), Review of wind simulation methods for horizontal-axis wind turbine analysis, *Technical report PNL-5903[R]*. Richland, WA: Battelle Pacific Northwest Laboratory.

Shen, W.Z., Mikkelsen, R., Sørensen, J.N. and Bak, C. (2005), "Tip loss corrections for wind turbine computations", *Wind Energy*, **8**(4), 457-475.

Shinozuka, M. (1971), "Simulation of multivariate and multidimensional random processes", *J. Acoust. Soc. Am.*, **49**(1-2), 357-368.

Shinozuka, M. and Jan, C.M. (1972), "Digital simulation of random process and its application", *J. Sound Vib.*, **25**(1), 111-128.

Shinozuka, M., Yun, C.B. and Seya, H. (1990), "Stochastic methods in wind engineering", *J. Wind Eng. Ind. Aerod.*, **36**(2), 829-843.

Simiu, E. and Scanlan, R.H. (1996), *Wind effects on Structures*, John Wiley & Sons, New York.

Sundar, R.M. and Sullivan, J.P. (1983), "Performance of wind turbines in a turbulent atmosphere", *Sol. Energy*, **31**, 567-575.

Veers, P.S. (1984), *Modeling stochastic wind loads on vertical - axis turbines*, *SAND83-1909*, Sandia National Laboratories, Albuquerque, NM.

Yang, J.N. (1972), "Simulation of random envelope processes", *J. Sound Vib.*, **25**(1), 73-85.

Yang, J.N. (1973), "On the normality and accuracy of simulated random processes", *J. Sound Vib.*, **26**(3), 417-428.

*CC*